Simple and Efficient Extrinsic Camera Calibration Based on A Rational Model

William Bourgeous, Lili Ma, Pengyu Chen, Zhen Song, and YangQuan Chen

Center for Self-Organizing and Intelligent Systems (CSOIS),
Dept. of Electrical and Computer Engineering, 4160 Old Main Hill,
Utah State University (USU), Logan, UT 84322-4160, USA.

***Abstract*— Calibration of the transformation between two planes, the image plane and the 2D platform, is important for applications where 2D metric information on the image plane is used to compute the 3D information in a world coordinate system. Efforts have been taken in computer vision literature to perform a full-scale camera calibration, including intrinsic and extrinsic parameters. For some applications, calibration of intrinsic parameters is not required as often as that of the extrinsic parameters. This paper addresses the problem of calibrating a camera's extrinsic parameters with respect to a 2D platform to which a camera is observing. A rational approximation method is proposed. Simulation and experimental results show that the proposed rational approximation method achieves comparable accuracy with the well-known homography-based approach. This work is motivated by our mobile sensor network project. Other relevant applications include vision-based metrology.**

***Index Terms*— Extrinsic parameter calibration, homography-based method, sensor networks.**

I. Introduction

With the growth of internet applications and the advance of mobile computing, wireless networking becomes a very important technology. Research has been done to increase the data bandwidth such that multimedia data can be transferred via wireless communication. However, there are applications that do not require a multi-mega bits per second bandwidth. Most of these low data-rate applications involve some sort of sensing cooperative work. These wireless communication networks are called Wireless Sensor Networks. A very thorough overview of the wireless sensor networks can be found in [1].

Our Mobile Actuator-Sensor Network (MAS-net) platform combines mobile robotics with the wireless sensor networks. The goal is to develop systems that collect and respond to data from spatially distributed diffusion processes. An extended application of this project can be in homeland security, where chemical, biological, radiological or nuclear (CBRN) terrorism can cause far more devastating damages. It is thus important to have a system that can respond and control the diffusion process of the harmful materials. Some research challenges and opportunities are presented in [2]. A preliminary result of a diffusion-based path planning is given in [3].

This work is supported in part by Utah State University SDL Skunk-Works Research Initiative Grant (2003-2005), CURI Grant (2005-2006) and NSF DDDAS/SEP Grant CMS-0540179. Corresponding author: Prof. YangQuan Chen, Center for Self-Organizing and Intelligent Systems, Dept. of Electrical and Computer Engineering, 4160 Old Main Hill, Utah State University, Logan, UT 84322-4160. **T**: (435)7970148, **F**: (435)7973054, **W**: `www.csois.usu.edu`, **E:** `yqchen@ece.usu.edu`.

A. MAS-net Project

A test bed has been built at CSOIS to observe a 2D diffusion process. The platform is a 92.7×141.25 square inch container, covered with transparent acrylic boards. Ten small Mica2-based robots, as shown in Fig. 1, are built to move on the platform [4].

Fig. 1. Ten Mica2-based robots for the MAS-net project.

The application scenario is to observe, detect and control the diffusion boundary when a 2D diffusion process, such as fog, is released into the platform. An overhead CCD camera is hung about 72 inches above the platform. The height of the camera is determined by the field of view of the camera. As will be described in Sec. II, the function of the camera is to identify each robot and give the position and orientation of the robot. The image processing is performed in a central computer, which also issues commands to the robots based on the sensor readings and processing. The platform is illustrated in Fig. 2.

B. Outline

The paper is organized as follows. Section II describes the function of the image processing module that identifies each robot and gives the robot's position and orientation. Section III describes the camera model and list notations that are used throughout this paper. Techniques that calibrate the coordinate transformation between the image plane and the 2D platform are given in Sec. IV, where our proposed rational approximation method is also presented. Section V shows our simulation and experimental results for the coordinate transformation calibration. Finally, section VI concludes the paper.

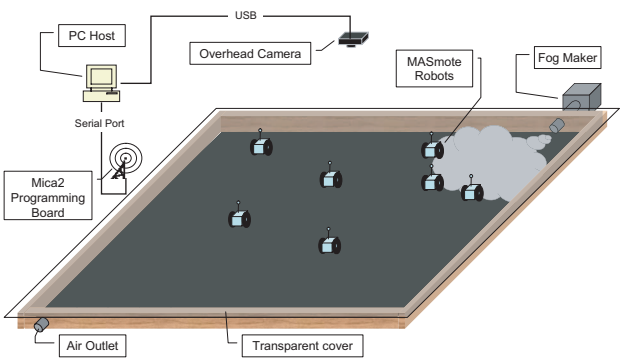

(a)

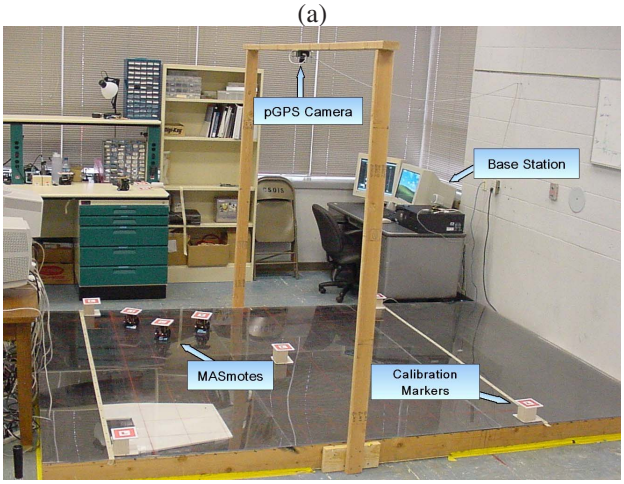

(b)

Fig. 2. Conceptual illustration of the test-bed (a) and the actual test-bed built (b) for the MAS-net project.

II. Image Processing

The image processing module is based on a modified ARToolKit [5]. The function of the image processing module is to provide position, orientation, and ID based on the markers on top of our robots. The image processing procedure is shown in Fig. 3 which includes:

- Color Segmentation: to extract the pixels that are of interests. This step can be understood as an image filter applied to the sample image based on colors.
- Marker Identification: to recognize and identify the markers on the robots. This work is based on the ARToolKit. Since the position and orientation detected by the ARToolKit are on the image plane in a pixel level, an additional step is needed to transform the processed metric information to the platform on which the robots are operating.
- Coordinate Transformation: to transform the extracted image coordinates to the world coordinates. Ideally, the camera needs to be aligned perfectly parallel to the 2D platform such that the effect of the projective projection can be minimized. However, this is difficult to achieve. Thus, an efficient and accurate calibration of the coordinate transformation is performed before using information obtained from the vision system.

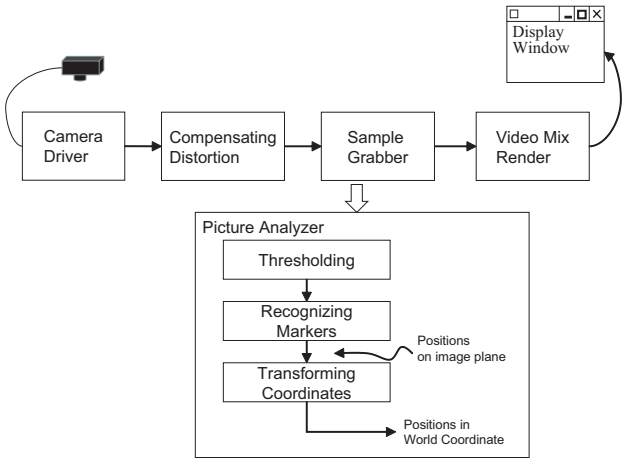

Fig. 3. Image processing module.

To provide more accurate pseudo GPS information of the robots, efforts have been taken in the above listed three steps. In this paper, we focus on the coordinate transformation. More specifically, we use "coordinate transformation" to refer to the calibration of the mapping from a metric information on the image plane to its corresponding metric information on the 2D platform.

In this paper, it is assumed that the camera's intrinsic parameters will not change as often as the camera's extrinsic parameters. Thus, it is reasonable to assume that the camera's intrinsic parameters are known during the calibration of the coordinate transformation. The camera model, lens distortion, and some general notations are described in Sec. III.

III. Notation and Camera Model

Using a camera's pinhole model, the projection from the 3D space to the image plane can be described by:

$$\lambda \begin{bmatrix} u \\ v \\ 1 \end{bmatrix} = \underbrace{\begin{bmatrix} \alpha & \gamma & u_0 \\ 0 & \beta & v_0 \\ 0 & 0 & 1 \end{bmatrix}}_{A_{\text{intr}}} \begin{bmatrix} R \mid \vec{t} \end{bmatrix} \begin{bmatrix} X^w \\ Y^w \\ Z^w \\ 1 \end{bmatrix}, \qquad (1)$$

where $(R, \vec{t})$ represents the transformation between the camera frame and the world coordinate system. The matrix A_{intr} denotes the camera's intrinsic matrix. $(\alpha, \gamma, \beta, u_0, v_0)$ are the camera's five intrinsic parameters, with (α, β) being two scalars in the two image axes, (u_0, v_0) the coordinates of the principal point and γ describing the skewness of the two image axes. The principal point is assumed to be at the center of distortion in this paper.

In (1), (u, v) is not the actually observed image point since virtually all imaging devices introduce certain amount of nonlinear distortions. Among the nonlinear distortions, radial distortion, which is performed along the radial direction from the center of distortion, has been recognized to be the most severe part. In the category of polynomial radial distortion modeling, the commonly used radial distortion function is suggested to be governed by the following polynomial equation

[6], [7]:

$$r_d = r+\delta_r = r\, f(r,\mathbf{k}) = r\,(1+k_1r^2+k_2r^4+k_3r^6+\cdots), \quad (2)$$

where $\mathbf{k} = [k_1, k_2, k_3, \ldots]$ is a vector of distortion coefficients. r and r_d can be defined either in the camera frame as:

$$r_{xy} = \sqrt{x^2+y^2}, \quad r_{dxy} = \sqrt{x_d^2+y_d^2}$$

with $x = X^c/Z^c$, $y = Y^c/Z^c$, or on the image plane as:

$$r_{uv} = \sqrt{(u-u_0)^2+(v-v_0)^2},$$
$$r_{duv} = \sqrt{(u_d-u_0)^2+(v_d-v_0)^2},$$

where the subscript $_d$ denotes the distorted version of the ideal projections. The subscripts $_{uv}$ and $_{xy}$ denote the quantities on the image plane and the camera frame, respectively. In this paper, coordinate transformation refers to the mapping from (x, y) to (X^w, Y^w), where (x, y) have been assumed to be distortion-compensated and transformed back to the camera frame (not in the pixel coordinates). Specific value of the lens's focal length f is not needed in the calibration of the coordinate transformation.

Suppose the transformation between the camera frame and the world coordinate system is described by:

$$P^c = RP^w + \vec{t}, \quad (3)$$

where P^w and P^c denote a point in the world coordinate system and the camera frame, respectively. R and $\vec{t}$ represent the transformation between these two frames. For simplicity, we can further assume that $Z^w = 0$ without loss of generality. Let the rotation about the X^w, Y^w, Z^w axes be (ω, ϕ, φ). The rotation matrix R becomes:

$$\begin{aligned} R &= R_z(\varphi)\, R_y(\phi)\, R_x(\varphi) \\ &= \begin{bmatrix} c\phi c\varphi & s\omega s\phi c\varphi - c\omega s\varphi & c\omega s\phi c\varphi + s\omega s\varphi \\ c\phi s\varphi & s\omega s\phi s\varphi + c\omega c\varphi & c\omega s\phi s\varphi - s\omega c\varphi \\ -s\phi & s\omega c\phi & c\omega c\phi \end{bmatrix} \quad (4) \end{aligned}$$

where c and s denote $\cos(\cdot)$ and $\sin(\cdot)$.

Notice that, the objective of the coordinate transformation is not to compute $[R, \vec{t}]$ specifically, but to find an accurate mapping from the metric information, (x, y) or (u, v) on the image plane, to (X^w, Y^w) on the 2D platform.

IV. Calibration of Camera's Extrinsic Parameters

Before any quantitative information from the vision system can be used, we have to know the relationship between the robot and the camera coordinate systems, in addition to the camera's intrinsic parameters [8]. Considerable efforts have been made on the development of effective and accurate algorithms to identify the camera's internal characteristics. Most works are focused on the complete camera calibration that involves calibrating both the intrinsic and extrinsic parameters [9]. However, for applications such as vision-based metrology and our case where the camera is used to provide pseudo GPS information, calibration of the camera's intrinsic parameters is not required as often as that of the extrinsic parameters. The extrinsic parameters need to be calibrated many times during the operating periods to compensate environmental noise and disturbance.

In this section, we present our efforts in calibrating the extrinsic parameters between the camera frame and the 2D platform using approximation methods [10] and the homography-based method [6]. Our proposed rational approximation method is presented in Sec. IV-B, which is motivated by the model presented in [10], but is shown to be able to achieve comparable accuracy with the well-known homography-based approach.

The following work assumes that the camera's intrinsic parameters $(\alpha, \gamma, \beta, u_0, v_0)$ are already given by an off-line calibration process, such as the camera calibration algorithm presented in [6]. It is also assumed that the ground surface, or the platform surface, is smooth. Note that the latter assumption is easy to satisfy in an indoor environment. In our project, customized patterns that are specifically designed for detections are used to speed up the image processing and provide satisfactory identification accuracy.

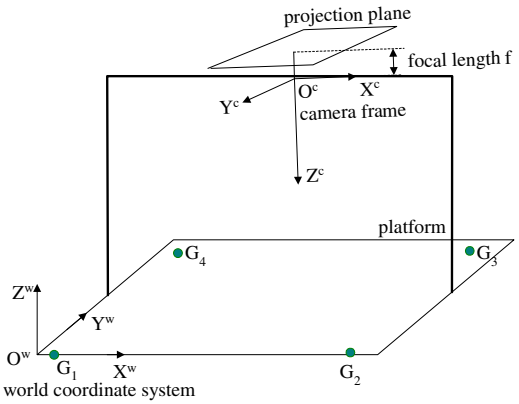

Fig. 4. Calibration of the coordinate transformation from the image plane to the 2D platform.

As illustrated in Fig. 4, a camera is mounted above the platform on which the robots are operating. The function of the camera is to identify the robots (either robots from different groups or different robots in the same group) and provide their positions and orientations. Ideally, the camera is to be placed at a position such that its camera frame, which is assumed to be identical to the image coordinate axes for simplicity, is parallel to the world coordinate system assigned on the platform. In this way, the metric information in the world coordinate system can be easily obtained from its corresponding metric information extracted from the image plane, since the perspective effect in the camera's modeling is minimized and the relationship between the two planes can be established using a scalar constant. However, due to the difficulty in achieving a perfect parallelism, using a scalar to model the relationship between the metric information on the two planes will not be accurate enough. This phenomenon is exaggerated when the distance from the camera to the platform becomes large, which is the case in our experimental setup where the camera needs to be placed well above the platform to provide global pseudo GPS information.

A. Approximation Method

The following approximation method has been applied to calibrate the coordinate transformation from the image plane to the 2D platform in [10]:

$$X^w = \sum_{j=0}^{m}\sum_{k=0}^{m} a_{jk}\, x^j\, y^k, \tag{5a}$$

$$Y^w = \sum_{j=0}^{m}\sum_{k=0}^{m} b_{jk}\, x^j\, y^k, \tag{5b}$$

where $P^w = [X^w, Y^w, 0]^T$ denotes a point in the world coordinate system at $Z^w = 0$. $[x, y]^T = [X^c/Z^c, Y^c/Z^c]^T$ denotes the normalized projection of P^w in the camera frame.

When $m = 1$, equations (5a) and (5b) become:

$$X^w = a_0 + a_1\, y + a_2\, x + a_3\, x\, y, \tag{6a}$$

$$Y^w = b_0 + b_1\, y + b_2\, x + b_3\, x\, y. \tag{6b}$$

The parameters $\vec{\alpha} = [a_0, a_1, a_2, a_3, b_0, b_1, b_2, b_3]^T$ can be solved in a least-square sense. That is, given a set of feature points P_i^w for $i = 1, 2, \ldots, n$ and their corresponding projections on the imaging surface $[x_i, y_i]^T$, find the best parameters $\vec{\alpha}$ such that the error in (6a) and (6b) are minimized.

Construct a matrix $\mathbf{D}$ and a vector $\vec{h}$ as:

$$\mathbf{D} = \begin{bmatrix} 1 & x_1 & y_1 & x_1\, y_1 & 0 & 0 & 0 & 0 \\ 0 & 0 & 0 & 0 & 1 & x_1 & y_1 & x_1\, y_1 \\ 1 & x_2 & y_2 & x_2\, y_2 & 0 & 0 & 0 & 0 \\ 0 & 0 & 0 & 0 & 1 & x_2 & y_2 & x_2\, y_2 \\ \vdots & \vdots & \vdots & \vdots & \vdots & \vdots & \vdots & \vdots \\ 1 & x_n & y_n & x_n\, y_n & 0 & 0 & 0 & 0 \\ 0 & 0 & 0 & 0 & 1 & x_n & y_n & x_n\, y_n \end{bmatrix}, \tag{7}$$

$$\vec{h} = [\, X_1^w \quad Y_1^w \quad X_2^w \quad Y_2^w \quad \ldots \quad X_n^w \quad Y_n^w \,]^T.$$

Then the least-square solution of

$$\mathbf{D}\,\vec{\alpha} = \vec{h} \tag{8}$$

is $\vec{\alpha} = \mathbf{D}^{-1}\vec{h}$ when $n = 4$. When $n > 4$, $\mathbf{D}$ becomes a $2n \times 8$ matrix. $\vec{\alpha}$ can be computed via pseudo inverse as $\vec{\alpha} = (\mathbf{D}^T\mathbf{D})^{-1}\mathbf{D}^T\vec{h}$.

B. Rational Approximation Method

Motivated from the observation that the polynomial $a_0 + a_1x + a_2y + a_3xy$ in (6a) can be represented by $(\kappa_1 x + \kappa_2)(\kappa_3 y + \kappa_4)$, where κ_i for $i = 1, 2, 3, 4$ are some constant scalars, it is straightforward to ask if a rational representation can be a better approximation since a rational function is rich in power series [7]. That is, consider:

$$X^w = \frac{\kappa_1 x + \kappa_2}{\kappa_5 x + 1} \cdot \frac{\kappa_3 y + \kappa_4}{\kappa_6 y + 1}. \tag{9}$$

However, the above equation is not linear in the six parameters c_i and a nonlinear method needs to be applied to find the optimized parameters. Alternatively, let us consider:

$$X^w = \frac{a_0 + a_1 x + a_2 y + a_3 xy}{1 + c_0 x + c_1 y + c_2 xy}, \tag{10a}$$

$$Y^w = \frac{b_0 + b_1 x + b_2 y + b_3 xy}{1 + d_0 x + d_1 y + d_2 xy}. \tag{10b}$$

Equations (10a) and (10b) are linear but require 14 calibration parameters as opposed to 8 parameters required in the previous method. Through simulation it was found that the cross terms of the rational method could be eliminated with little loss of accuracy. This simplified rational method requires only 10 calibration parameters which make it simple to use, see equation (11).

$$X^w = \frac{a_0 + a_1 x + a_2 y}{1 + c_0 x + c_1 y}, \tag{11a}$$

$$Y^w = \frac{b_0 + b_1 x + b_2 y}{1 + d_0 x + d_1 y}. \tag{11b}$$

Let

$$\vec{\alpha} = [a_0, a_1, a_2, c_0, c_1, b_0, b_1, b_2, d_0, d_1]^T.$$

Equation (11) can be written as:

$$\begin{bmatrix} X^w\tilde{N}^T & -1 & \tilde{N}^T & \mathbf{0} & 0 & \mathbf{0} \\ \mathbf{0} & 0 & \mathbf{0} & Y^w\tilde{N}^T & -1 & \tilde{N}^T \end{bmatrix} \vec{\alpha} = -\begin{bmatrix} X^w \\ Y^w \end{bmatrix}, \tag{12}$$

where $\tilde{N}$ stands for $[x, y]^T$. Where we have n points and n equations the parameters $\vec{\alpha}$ can be computed using the least-square method.

C. Homography-Based Method

The well-known homography-based method is also used to calibrate the transformation between the two planes. From (3) and assuming that $Z^w = 0$, we have:

$$\begin{bmatrix} X^c \\ Y^c \\ Z^c \end{bmatrix} = \begin{bmatrix} r_{11} & r_{12} & t_1 \\ r_{21} & r_{22} & t_2 \\ r_{31} & r_{32} & t_3 \end{bmatrix} \begin{bmatrix} X^w \\ Y^w \\ 1 \end{bmatrix}. \tag{13}$$

Assume further that the camera's focal length $f = 1$. Thus, we have:

$$\begin{aligned} x &= \frac{X^c}{Z^c} = \frac{r_{11}X^w + r_{12}Y^w + t_1}{r_{31}X^w + r_{32}Y^w + t_3}, \\ y &= \frac{Y^c}{Z^c} = \frac{r_{21}X^w + r_{22}Y^w + t_2}{r_{31}X^w + r_{32}Y^w + t_3}. \end{aligned} \tag{14}$$

Let $\vec{\alpha} = [r_{11}, r_{12}, t_1, r_{21}, r_{22}, t_2, r_{31}, r_{32}, t_3]^T$. Equation (14) can be rewritten as:

$$\begin{bmatrix} \tilde{M}^T & \mathbf{0}^T & -x\tilde{M}^T \\ \mathbf{0}^T & \tilde{M}^T & -y\tilde{M}^T \end{bmatrix} \vec{\alpha} = \mathbf{0}, \tag{15}$$

where $\tilde{M}^T$ denotes $[X^w, Y^w, 1]^T$. When we are given n points, we have n above equations, which can be written in a matrix equation as $L\vec{\alpha} = \mathbf{0}$, where the dimension of L is $2n \times 9$. The solution of $\vec{\alpha}$ is well known to be the right singular vector of L associated with the smallest singular value.

V. Validation

This section covers three tiers of validation testing: simulation, experimentation and platform integration.

A. Simulation

We first study simulations where there is no measurement noise in the feature extractions and the camera's intrinsic parameters are perfectly known. It has been observed that using more calibration points will always produce better performance. The above is intuitive and consistent with the theoretical analysis. However, it is impractical to set up and maintain a large number of calibration points. A comparison is performed between each of the three methods outlined in section IV.

Throughout the remainder of this paper units of radians and meters are consistently used. The true values of $\vec{t}$ and (ω, ϕ, φ) in (3) and (4) are set to be:

$$\begin{aligned}(\omega, \phi, \varphi) &= (\pi - \pi/40, \pi/40, -\pi/40),\\ \vec{t} &= [-1.5, 1, 2]^T.\end{aligned} \tag{16}$$

Fig. 5 shows the position estimation errors (2-norm) on the simulation platform using the approximation method, our proposed rational approximation method in (11) and finally the homography method. Each method uses only five points to calculate the calibration parameters, thus the comparison is fair. To test the calibration, the platform is evenly partitioned into small grids and the points on the grids are used as the testing set. It can be observed from Fig. 5(a) that the errors are not evenly distributed but increasing near the center of the platform when using the approximation method. Notice that in both Fig. 5(b) and Fig. 5(c) the error distributions is remarkably small, on the order of 10^{-15}. Fig. 5(b) shows that the error distribution is relatively even compared to that in Fig. 5(a). An interesting phenomenon is that the errors around the center of the platform are quenched down when using the rational approximation method but errors around the boundary of the platform might increase. From this simulation we conclude that our rational approximation method improves accuracy over that of the original approximation method and is comparable to the traditional homography-based method.

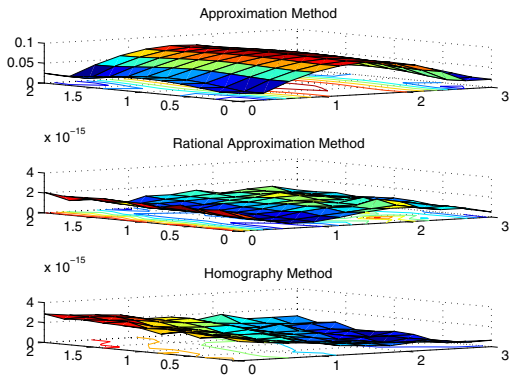

Fig. 5. Simulation based position error distribution comparison.

The maximum, and mean position error corresponding to the three cases shown in Fig. 5 are:

$$\text{Fig. 5}: \begin{cases} & \text{Max} & \text{Mean}: \\ (a): & 0.0804 & 0.0500, \\ (b): & 0.2054 \times 10^{-14} & 0.1108 \times 10^{-14}, \\ (c): & 0.2855 \times 10^{-14} & 0.1289 \times 10^{-14} \end{cases} \tag{17}$$

It is observed from (17) that our proposed approach, shown in case (b), achieves the lowest mean error.

B. Experimentation

To test the simulation results another comparison of methods is made using data from an actual camera on a scaled down test platform. The experimental results are presented in this section. In this experiment, a calibration target full of patterns is placed at a position roughly one-tenth of the actual distance in the real platform, as shown in Fig. 6. Thus, the actual position error can be inferred from the results given in this section by a multiplicity of ten. This experiment differs from the simulations presented in Sec. V-A, in that, the number of calibration points is increased along with increased measurement noise from feature extraction and from the camera intrinsic modeling.

Fig. 6. Portion of the calibration target with patterns.

Fig. 7 shows the experimental position error using the approximation, rational approximation and homography-based methods, respectively, where the format of Fig. 7 is the same as that in Fig. 5. Comparison between the figures indicate the same conclusions drawn from the simulation. That is, our proposed rational approximation function achieves the best accuracy when compared with the others.

The maximum and mean position error corresponding to Fig. 7 are respectively:

$$\text{Fig. 7}: \begin{cases} & \text{Max} & \text{Mean}: \\ (a): & 0.0020 & 0.0010, \\ (b): & 0.0007 & 0.0003, \\ (c): & 0.0009 & 0.0004 \end{cases} \tag{18}$$

It is clear from the above data that the proposed rational approximation method can achieve comparable, or even better, estimation accuracy than homography-based approach in a testing environment.

C. Implementation

Vision based software is computationally intensive which can impose physical limits on our system. For example, delays between pseudo GPS position update messages will limit the performance of the individual robots and can cause instability.

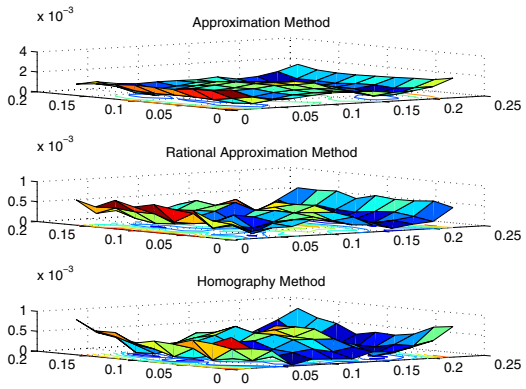

Fig. 7. Experimentation based position error distribution comparison.

The ultimate goal of this work is to implement the simplest and most accurate calibration method into our MAS-net platform to achieve the best system performance.

A final test of our proposed rational approximation method is a full scale, side by side comparison performed on our MAS-net platform. The increased complexity of implementing the homograpy-based method excludes it form this comparison. To achieve the best possible results on the platform a 2.4 meter square was marked by chalklines and a five point calibration was used to obtain the 10 calibration parameters needed, as shown in Fig. 8.

Fig. 8. Platform calibration method.

The maximum and mean position error corresponding to Fig. 9 are:

$$\text{Fig. 9}: \begin{cases} & \text{Max} & \text{Mean}: \\ (a): & 0.0279 & 0.0132, \\ (b): & 0.0196 & 0.0106. \end{cases} \tag{19}$$

The physical difficulties of accurately measuring the placement of markers on the full-scale platform limit the degree of accuracy possible in this experiment. However, it is clear that some modest improvement in calibration accuracy is achieved by using the proposed simple rational approximation method in place of the current approximation method.

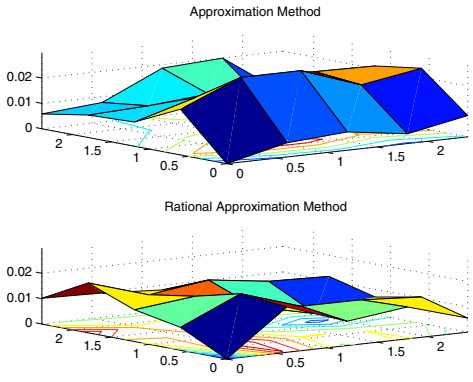

Fig. 9. Implementation position error distribution on the platform.

VI. Concluding Remarks

In this paper, a rational approximation method is proposed to calibrate the coordinate transformation from a camera's image plane to a 2D platform. Both approximation-based methods and a homography-based approach are studied and compared in a fair manner with an equal number of calibration points. The simulation and experimental results show that our proposed rational approximation method can achieve comparable estimation accuracy with the well-known homography-based approach but has the advantage of a simpler implementation.

References

[1] E. H. Callaway, *Wireless Sensor Networks: Architectures and Protocols*. 2000 N.W. Corporate Blvd., Boca Raton, Florida 33431: CRC Press LLC, 2003.

[2] K. L. Moore and Y. Chen, "Model-based approach to characterization of diffusion processes via distributed control of actuated sensor networks," in *IFAC Symposium of Telematics Applications in Automation and Robotics, Helsinki University of Technology Espoo, Finland*, 2004.

[3] Y. Chen, K. L. Moore, and Z. Song, "Diffusion based path planning in mobile actuator-sensor networks (mas-net) - some preliminary results," in *Proc. of SPIE Conf. on Intelligent Computing: Theory and Applications II, part of SPIEs Defense and Security, Orlando, FL*, 2004.

[4] Z. Wang, Z. Song, P. Chen, A. Arora, K. L. Moore, and Y. Chen, "Masmote - a mobility node for mas-net (mobile actuator sensor networks)," in *IEEE Int. Conf. on Robotics and Biomimetics, Shengyang, China*, 2004.

[5] U. of Washington, "Artoolkit," Human Interface Technology Laboratory, http://www.hitl.washington.edu/artoolkit/, 2004.

[6] Z. Zhang, "Flexible camera calibration by viewing a plane from unknown orientation," *IEEE International Conference on Computer Vision*, pp. 666–673, Sept. 1999.

[7] L. Ma, Y. Chen, and K. L. Moore, "Rational radial distortion models of camera lenses with analytical solution for distortion correction," *International Journal of Information Acquisition*, vol. 1, no. 2, pp. 135–147, June 2004.

[8] Y. L. Chang. and J. K. Aggarwal, "Calibrating a mobile camera's extrinsic parameters with respect to its platform," in *Proceedings of the 1991 IEEE International Symposium on Intelligent Control*, Aug. 13-15 1991, pp. 443–448.

[9] F.-Y. Wang, "A simple and analytical procedure for calibrating extrinsic camera parameters," *IEEE Transactions on Robotics and Automation*, vol. 20, no. 1, pp. 121–124, Feb. 2004.

[10] C.-C. Wong, C.-P. Huang, B.-C. Lin, and Y.-S. Huang, "Position correction in the image process of robot soccer game," in *The Seventh Conference on Artificial Intelligence and Applications (TAAI2002), Taichung, Taiwan*, 2002, pp. 684–689.